SCIENTIFIC REPORTS

OPEN

SUBJECT AREAS:
ELECTRONIC PROPERTIES AND MATERIALS
SUPERCONDUCTING PROPERTIES AND MATERIALS
STRUCTURE OF SOLIDS AND LIQUIDS

Received
22 May 2014

Accepted
15 July 2014

Published
30 July 2014

Correspondence and requests for materials should be addressed to Z.R. (zamra51@ifm.liu.se)

Novel superconducting skutterudite-type phosphorus nitride at high pressure from first-principles calculations

Zamaan Raza[1,2], Ion Errea[1,3,4], Artem R. Oganov[5,6,7,8] & A. Marco Saitta[1,2]

[1]Sorbonne Universités, UPMC Univ. Paris 06, UMR 7590, Institut de Minéralogie, de Physique des Matériaux et de Cosmochimie (IMPMC), F-75005 Paris, France, [2]CNRS, UMR 7590, Institut de Minéralogie, de Physique des Matériaux et de Cosmochimie (IMPMC), F-75005 Paris, France, [3]Donostia International Physics Center (DIPC), Manuel de Lardizabal pasealekua 4, 20018 Donostia-San Sebastián, Basque Country, Spain, [4]IKERBASQUE, Basque Foundation for Science, 48011, Bilbao, Spain, [5]Department of Geosciences, State University of New York, Stony Brook, NY 11794-2100, USA, [6]Center for Materials Design, Institute for Advanced Computational Science, State University of New York, Stony Brook, NY 11794-2011, USA, [7]Moscow Institute of Physics and Technology, 9 Institutskiy Lane, Dolgoprudny City, Moscow Region, 141700, Russian Federation, [8]Northwestern Polytechnical University, Xi'an, 710072, China.

State of the art variable composition structure prediction based on density functional theory demonstrates that two new stoichiometries of PN, PN_3 and PN_2, become viable at high pressure. PN_3 has a skutterudite-like *Immm* structure and is metastable with positive phonon frequencies at pressures between 10 and 100 GPa. PN_3 is metallic and is the first reported nitrogen-based skutterudite. Its metallicity arises from nitrogen p-states which delocalise across N_4 rings characteristic of skutterudites, and it becomes a good electron-phonon superconductor at 10 GPa, with a T_c of around 18 K. The superconductivity arises from strongly enhanced electron-phonon coupling at lower pressures, originating primarily from soft collective P-N phonon modes. The PN_2 phase is an insulator with *P2/m* symmetry and is stable at pressures in excess of 200 GPa.

High pressure synthesis offers a route to new materials with promising technological applications such as superconductors[1–4] as well as to compounds with unexpected stoichiometries[5]. New theoretical structure prediction techniques[6–9] have been used to identify novel superconductors by applying pressure to stoichiometries that form phases without the properties of superconductivity, metallicity or even stability at atmospheric pressure[10–15]. In spite of their great potential, nitride-based materials remain relatively unexplored due to the high stability of nitrogen molecules at ambient pressure; the strong N≡N triple bond results in a high kinetic barrier to polymerisation, thus extreme temperatures and pressures are required to synthesise many nitrides. However, at high pressures, the physical and chemical properties of nitrogen change substantially, allowing the formation of new polymeric crystalline phases[16] and the possibility of forming new nitrogen-based superconducting crystals.

Nitride-based superconductors were among the first discovered, and include examples with remarkably high superconducting critical temperatures (T_c), such as NbN (14.7 K)[17] and β-HfNCl (25.5 K)[18]. However, in both instances, the superconductivity does not originate from the nitrogen atoms[19], and the XNCl family of layered compounds have been proposed to be unconventional superconductors[20].

Another important example of superconductivity in pnictogen-based compounds involves the skutterudites, though, as far as we know, no nitrogen-based skutterudite has been found yet. They have the empirical formula TX_3, where T is typically a transition metal and X is a pnictogen. They form a low density body-centred cubic $Im\bar{3}$ lattice consisting of dodecahedral cages (Fig. 1). This cage can be filled with a guest atom to form MT_4X_{12},potentially changing the properties of the material, making it semiconducting[21], paramagnetic[22],superconducting[23] or even thermoelectric[24].They are also characterised by square X_4^{4-} groups connecting the cages, which are thought to influence electrical conductivity and superconductivity[25]. Filled skutterudite superconducting materials have been synthesised under pressure[26], and found to have high T_c values, for example $LaRu_4As_{12}$ with T_c = 10.3 K[26] and $La_{0.6}Rh_4P_{12}$ with T_c = 17 K, the highest known among metal phosphides[27]. It has been shown that although the guest atom in filled skutterudites stabilises the lattice, the superconductivity is an intrinsic property of the T_4X_{12} framework[28,29].

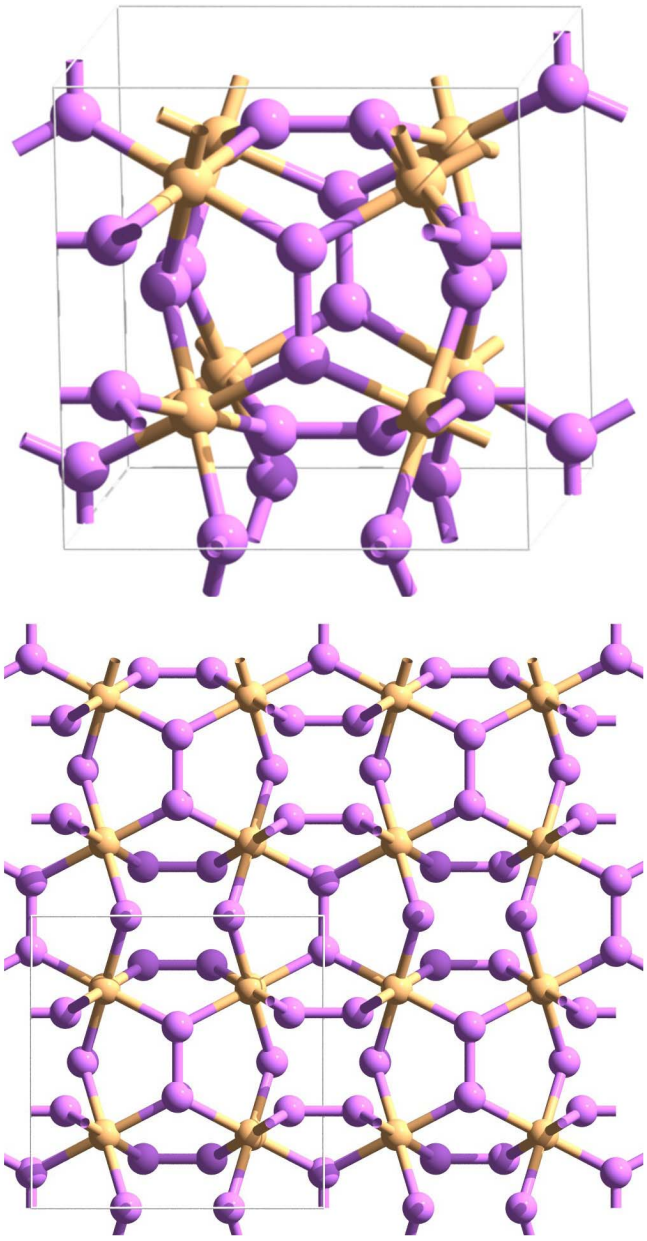

Figure 1 | The skutterudite-like *Immm* structure of PN_3 in its body-centred orthorhombic conventional cell. The skutterudite structure has $Im\bar{3}$ symmetry, but the PN_3 phase is characterised by an orthorhombic distortion. Phosphorus atoms are six-coordinated in both cases. Phosphorus atoms are yellow and nitrogen atoms purple.

In this article we perform a systematic search for thermodynamically stable phosphorus nitrides under pressure using evolutionary structure prediction and density functional theory (DFT). Beyond the only known stable phosphorus nitride, P_3N_5, which forms a variety of pressure-dependent phases[30–33], we find that a novel phosphorus nitride skutterudite (PN_3) containing six-coordinated phosphorus can be formed at undemanding pressures (~10 GPa). PN_3 is the first reported nitrogen-based skutterudite. It is metallic, metastable and dynamically stable between 10 and 100 GPa. Although it is unstable at ambient pressure, it may be possible to stabilise it using off-stoichiometry doping with a guest species at the centre of the cage, as with other skutterudite superconductors. PN_3 is a good superconductor with a T_c of around 18 K at 10 GPa, higher than for any known skutterudite. We also report the discovery of a new insulating phase with PN_2 stoichiometry, which is stable above 200 GPa.

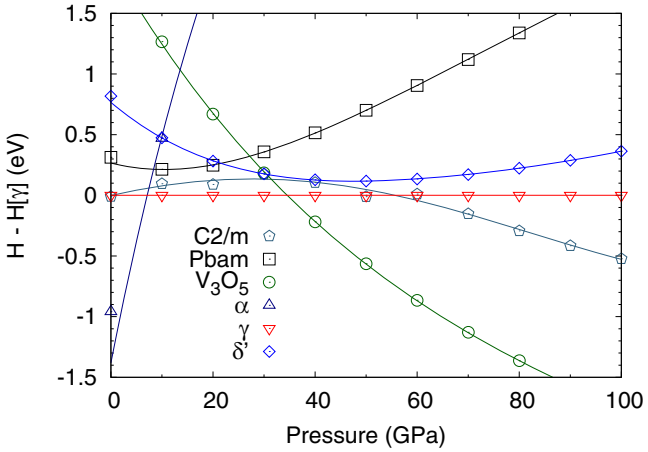

Figure 2 | Enthalpy per formula unit as a function of pressure for the best phases with the P_3N_5 stoichiometry.

Results

High pressure phosphorus nitride structures. In the first instance, fixed composition searches were performed using one and two formula units of P_3N_5 at pressures of 25 GPa, 50 GPa, 100 GPa and 200 GPa, yielding the *Imm*2 γ-phase at lower pressures, and the previously predicted *C*2/*c* oxyvanite phase at high pressures, in agreement with the findings of Dong *et al.*[34] The recovery of an experimentally verified phase in addition to a structure predicted through chemical intuition is a reassuring vindication of the USPEX code. According to the results presented in Fig. 2, the α phase, which is stable at ambient pressure, undergoes a transition to the γ phase at around 7 GPa, which transforms to the oxyvanite phase at 34 GPa. The previously predicted δ' phase[35] is at least 0.2 eV higher in enthalpy than γ.

Variable composition searches were performed at 100 GPa in order to identify potential stable stoichiometries; these were followed by fixed composition searches for the best stoichiometries at pressures of 25 GPa, 50 GPa, 100 GPa and 200 GPa using PN_3, PN_2, P_3N_4, P_3N_5 and PN. The resulting convex hull is shown in the

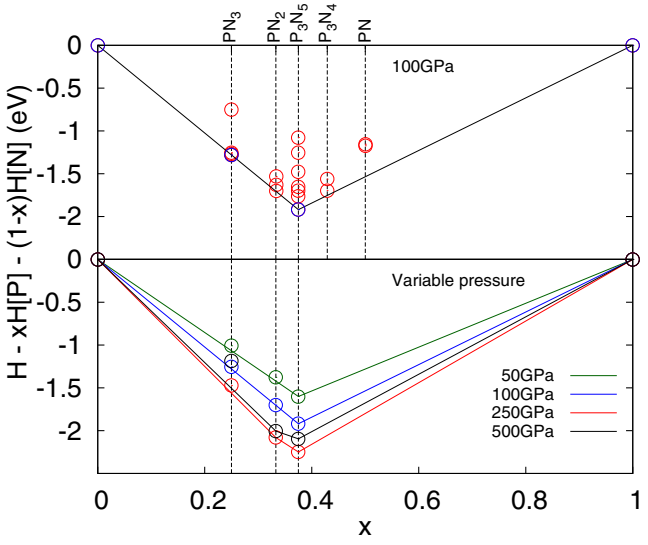

Figure 3 | Convex hull for the P_xN_{1-x} system at 100 GPa (top) and at different pressures (bottom). H is the enthalpy per atom of the generated structure, H[P] the enthalpy per atom of the stable phosphorus phase (simple hexagonal phosphorus at 100 GPa) and H[N] is the enthalpy per atom of the stable nitrogen phase (cubic gauche nitrogen at 100 GPa). The lower panel only includes the *Immm*-PN_3, *P*2/*m*-PN_2 and oxyvanite-P_3N_5 structures.

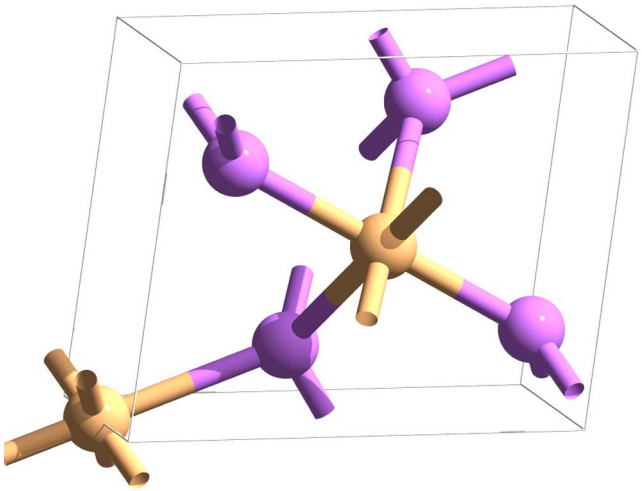

Figure 4 | The *P2/m* structure of PN_2, which becomes stable at pressures of above 200 GPa.

upper panel of Fig. 3, illustrating the most stable compositions: PN_3, PN_2 and P_3N_5. The enthalpies of the most interesting structures are plotted at different pressures in the lower panel. A new insulating *P2/m* phase of PN_2 (structure in Fig. 4 and electronic density of states in Fig. 5) becomes stable with respect to N and P_3N_5 at pressures in excess of 200 GPa, while the best PN_3 structure (*Immm*) is very close to the hull below 100 GPa. It is noteworthy that both new structures consist of octahedral PN_6 units, containing octahedral six-coordinated phosphorus atoms; this was unprecedented until a pressure induced transition to six-coordinated phosphorus was observed in $AlPO_4$ as a densification mechanism[36]. The structural parameters for these two new structures are listed in Table I.

The *Immm*-PN_3 skutterudite. The skutterudite-like PN_3 is formed from dodecahedral cages (Fig. reffig:Immm-structure) consisting of six-coordinated phosphorus atoms at the vertices of a cuboid, with the faces occupied by N_2 pairs, forming pentagonal rings. In contrast with all other known and predicted PN structure, the nitrogen atoms are all three-coordinated, compared with the γ, oxyvanite and new *P2/m* phases, which contain both three- and four-coordinated nitrogens. Surprisingly, the N–N bonds are extremely short; at 100 GPa, they are 1.28 Å, increasing to 1.30 Å at 10 GPa. No other structures were found with such a short bond length. As the pressure decreases, the orthorhombic distortion in the *Immm* cell becomes more pronounced in the *b* direction, causing the structure to break down; it is likely that this is thermodynamically favourable since the N_2 units are very close in geometry to their configuration in the gas phase. However, the structure is dynamically stable with well-defined positive phonons at pressures as low as 10 GPa. Thus the possibility remains that the skutterudite structure may be synthesised at moderate pressures.

MX_3 skutterudites are also characterised by six square X_4 rings in the conventional 32-atom cell. In PN_3, these rings are rectangular rather than square as a result of the orthorhombic distortion, but can be discerned as pairs of N_2 units separated by 1.9 Å at 100 GPa, which could be either a weak bond or a non-bonding contact. A Bader analysis reveals that the nitrogens have little ionic character, with a charge of 0.065 to 0.075*e*. These X_4 rings have been shown to give rise to conduction and superconductivity in other skutterudites, namely CoP_3 and NiP_3[37] and $LaFe_4P_{12}$[25].

PN_3 is metallic throughout its stable pressure range. There is a distinct set of three bands (Fig. 6) dispersing from approximately 1 eV below ϵ_F to 2 eV above ϵ_F responsible for the conductivity. The partial density of states (Fig. 6) demonstrates that the dominant

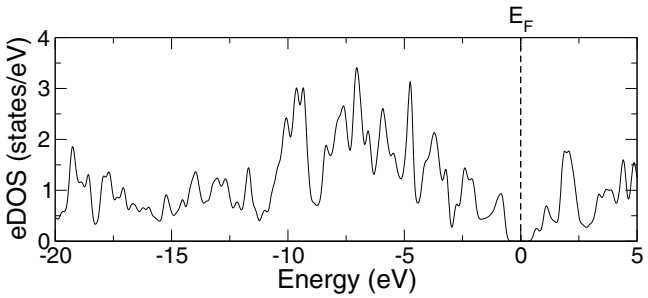

Figure 5 | Electronic density of states of the *P2/m* phase at 200 GPa.

contribution to the conducting bands arises from nitrogen 2p atomic orbitals. It is interesting to note that in electronic structure calculations of other metallic skutterudites, namely CoP_3 and NiP_3, the highest occupied bands consist of phosphorus centred p-orbitals[37], which occupy analogous positions to nitrogen in PN_3, phosphorus being isoelectronic to nitrogen.

The three bands around the Fermi level were projected onto maximally localised Wannier functions (MLWF), as illustrated in Fig. 7. The Wannier projections have p-orbital-like symmetry, but are delocalised across N_2 pairs which form adjacent skutterudite N_4 rings, accounting for the conductivity.

Phonon spectra and electron-phonon coupling in the *Immm*-PN_3 skutterudite. The phonon spectra of PN_3 (Fig. 8) are characterised by two groups of modes; firstly dispersive low-energy modes that involve collective vibrations of P and N atoms. These modes are separated from the second group, high-energy Einstein-like modes, primarily corresponding to vibrations of the short N−N bonds, by a distinct gap. As the pressure is lowered, the acoustic modes and some low-energy optical modes related to distortions of the whole dodecahedral cage are softened. This gives rise to a structural instability at ambient pressure as the lowest energy mode at the X and R point acquire an imaginary frequency. The instability is related to the decomposition of PN_3 and the formation of N_2 pairs. Structurally, this is manifested as the formation of PN "sheets" enclosing N_2 molecules, and is reflected by significant changes in the phonon dispersion. However, at 10 GPa the phonon spectrum does not display any imaginary frequencies and the crystal structure is dynamically stable.

The electron-phonon coupling constant λ, calculated from equation (3), scales linearly with the density of states at the Fermi level and is inversely proportional to the square of the phonon frequencies. Its calculated values are presented in Table II and the Eliashberg functions are plotted in Fig. 9. At all pressures studied, the eDOS at ϵ_F remains high due to the presence of weakly dispersive bands in the vicinity of the Fermi level (Fig. 6). This ensures a large electronic contribution to the Eliashberg functions coming from the double electronic Dirac delta in equation (1). Thus, the evolution of λ under pressure is mostly determined by the evolution of the phonon spectra.

At 10 GPa the electron-phonon coupling constant reaches a remarkable value of 1.05. The low-energy modes ($<$400 cm^{-1}) contribute more strongly to λ due to their low frequencies. This is evidenced by the strong contribution of the low-energy part of the Eliashberg function to λ, demonstrated in Fig. 9. The contribution to λ of the lowest energy acoustic mode at the R special point is particularly large. At 20 GPa, the electron-phonon coupling decreases as low-frequency modes gain energy. This causes the strong peaks in $\alpha^2F(\omega)$ at low energy to shift to higher frequencies and thus reduces their contribution to λ. At higher pressures, the energy of the lowest energy acoustic mode at R is strongly increased and, consequently, its contribution to λ is strongly suppressed, indu-

Table I | Structural parameters for the two new PN phases

Phase	Pressure (GPa)	Lattice *a*, *b*, *c* (Å) α, β, γ (°)	Wyckoff position		Atomic coordinates (fractional)		
PN_3	100	5.607 5.830 5.684	8*k*	P	0.2500	0.2500	0.2500
Immm		90.0 90.0 90.0	8*n*	N	0.3248	0.1104	0.0000
			8*l*	N	0.0000	0.6838	0.8820
			8*m*	N	0.8867	0.0000	0.3323
PN_2	200	3.324 2.392 4.011	1*b*	P	0.0000	0.5000	0.0000
P2/m		90.0 96.636 90.0	1*g*	P	0.5000	0.0000	0.5000
			2*m*	N	0.2752	0.0000	0.1459
			2*n*	N	0.1778	0.5000	0.6075

cing a considerable reduction of the electron-phonon coupling constant.

Using the computed values of the electron-phonon coupling constant, we estimated the superconducting T_c using the standard values of $\mu^* = 0.10$ and $\mu^* = 0.13$ for the Coulomb pseudopotential in equation (2). These values are summarised in Table II. T_c reaches 18.6 K for $\mu^* = 0.10$ at 10 GPa, a high value for an electron-phonon coupling superconductor. Using $\mu^* = 0.13$, a slightly lower but similar 16.1 K value is obtained, showing that for large values of λ T_c is weakly dependent on μ^*. The evolution of T_c is consistent with the pressure dependence of λ and both are suppressed at high pressures.

Inclusion of a guest atom in the skutterudite lattice. Filled skutterudites are of particular interest for their potential thermoelectric properties. If the void in a skutterudite cage is significantly larger than the guest atom, then the vibrational modes of the guest atom are expected to be strongly anharmonic, resulting in "rattling modes"[24]. These modes tend to reduce thermal conductivity by scattering the phonons responsible for heat transport[38] and, consequently, enhance the figure of merit of thermoelectric materials[39]. We now turn to the question of whether the skutterudite remains stable when it hosts such a guest atom.

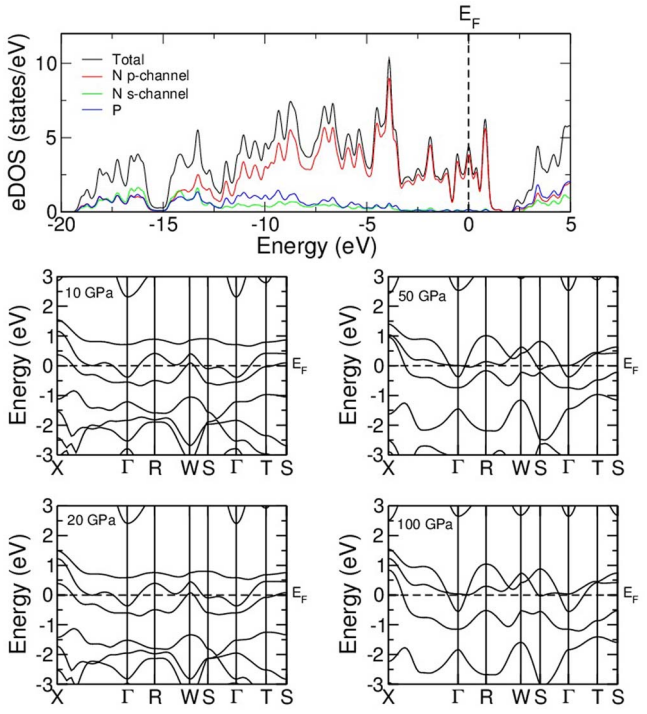

Figure 6 | Electronic structure of the *Immm* PN_3 phase. The electronic density of states (top panel) is decomposed into contributions from P atoms, N 2s electons and N 2p electrons. The band structure near the Fermi level is displayed at 10 GPa, 20 GPa, 50 GPa and 100 GPa.

It should be noted that the cage in PN_3 is considerably smaller than for other skutterudites, which are large enough to hold atoms such as barium, which has a covalent radius of 2.53 Å. PN_3 has a body-centred orthorhombic lattice at lower pressures, in contrast with most skutterudites which are body-centred cubic; the distance between the body centre of the cage and the closest point on the surface of the cage (specifically, the midpoint of a N_2 bond) is 1.81 Å, compared with 2.79 Å for $CoAs_3$. This greatly limits the choice of guest atom to smaller species such as hydrogen, lithium and beryllium.

A beryllium atom proved to be too large, resulting in imaginary frequencies throughout the Brillouin zone. A lone hydrogen atom was too thermodynamically unstable to occupy the body centre of the lattice, drifting towards a phosphorus atom during geometry optimisation and breaking the *Immm* symmetry. The phonon dispersion for PN_3 with a lithium guest has a soft mode at the X special point, and is therefore not stable; this was the case through the pressure range 10–100 GPa. In conclusion, it seems there is no stable XP_4N_{12} filled skutterudite.

The inclusion of a guest atom and a reduction of the external pressure have a similar effect on the atomic structure: the guest atom forces the cage to expand, just as the structure loses its dynamical stability as the lattice parameter increases at pressures below 10 GPa. It may be possible to stabilise the structure by doping the system with, for example, one lithium atom per eight conventional cells (i.e. a $2 \times 2 \times 2$ supercell), although this would necessitate phonon calculations that would be prohibitively expensive.

Discussion

In conclusion, we used density functional theory coupled with evolutionary structure prediction to explore the variable composition configuration space of phosphorus nitride. We identified a new stable stoichiometry, insulating PN_2 with *P2/m* symmetry, at pressures in excess of 200 GPa, and a fascinating new metastable structure, PN_3, which is dynamically stable between approximately 10 and 100 GPa.

The PN_3 structure has *Immm* symmetry, belongs to the $Im\bar{3}$ skutterudite class of compounds, and is the first to contain nitrogen as

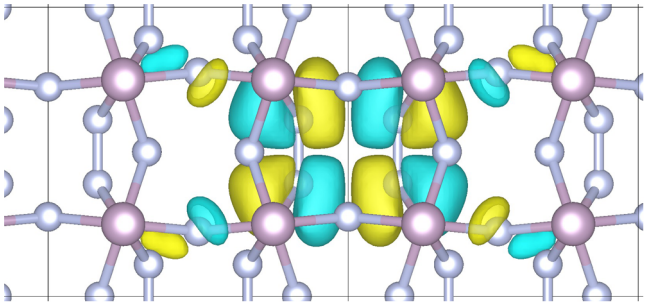

Figure 7 | A MLWF projection of the states from 1 eV below to 2 eV above ϵ_F at 100 GPa The orbital is spread over skutterudite N_4 rings, giving rise to electronic conductivity.

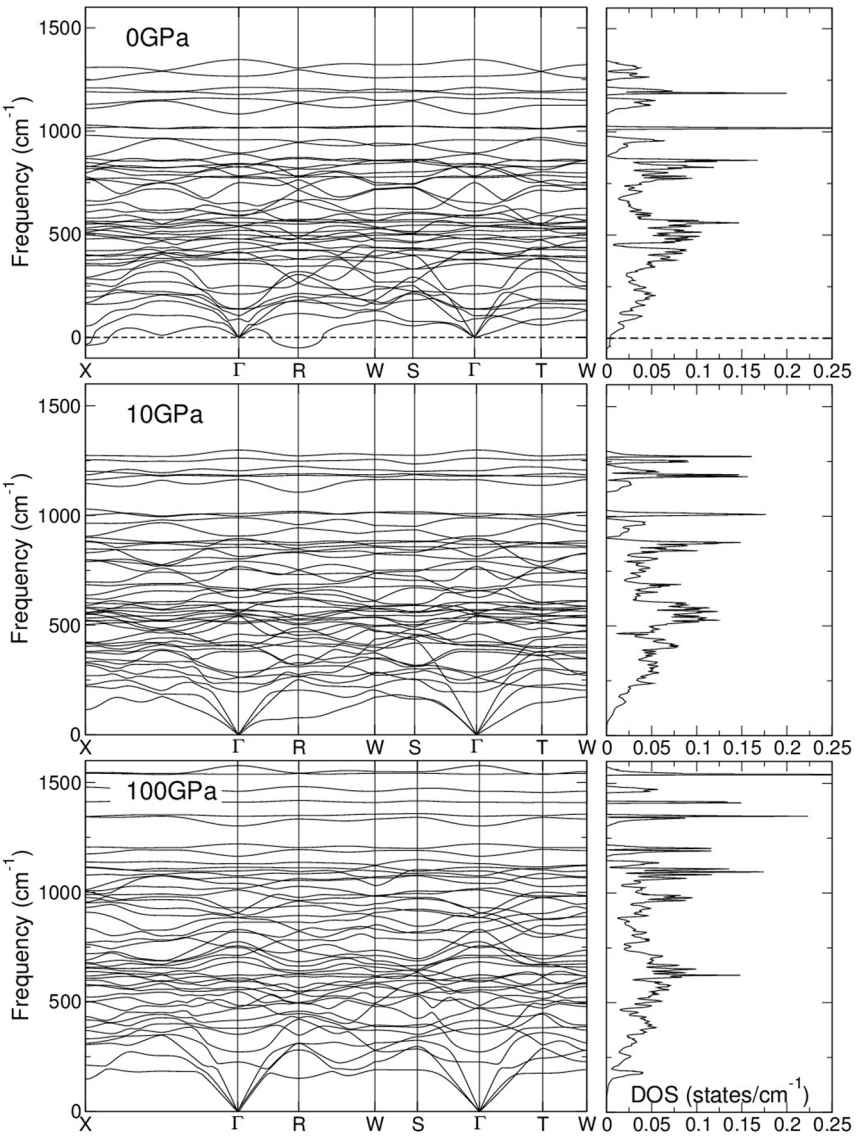

Figure 8 | Phonon dispersion and phonon density of states for the *Immm* phase at 0 GPa, 10 GPa and 100 GPa.

pnictogen. It is characterised by an orthorhombic distortion, the extent of which increases as the pressure is decreased. Skutterudite-PN_3 is metallic throughout the range of pressures examined, 10–100 GPa, its electrical conductivity arising from the delocalisation of nitrogen p-states across N_4 rings. Most significantly, it becomes a good electron-phonon superconductor with a T_c of around 18 K at 10 GPa due to strong electron-phonon coupling with low-frequency phonon modes. At higher pressures the superconducting T_c is suppressed as low-energy acoustic modes gain energy. The superconducting behavior of PN_3 is comparable to other high-pressure superconductors such as Te, Li and S, where the evolution of T_c under pressure is determined by the behavior of low-energy phonon modes, and is enhanced close to dynamical instabilities[40–42].

The phonon dispersion at 10 GPa shows no sign of instability, opening the door to the possibility of its synthesis, perhaps by chemical synthesis from precursors in the correct ratio, or thin film deposition on a substrate with a similar lattice parameter. Furthermore, although the dodecahedral cage is too small to host one guest atom (H, Li, Be) per primitive cell, it may be possible to stabilise the PN_3 lattice at ambient pressure using off-stoichiometry doping with a guest species.

Table II | Calculated λ, ω_{log} and T_c values for the *Immm*-PN_3 skutterudite. T_c is calculated with two different values for the Coulomb pseudopotential μ^*

P (GPa)	λ	ω_{log}(meV)	$T_c[\mu^* = 0.10]$(K)	$T_c[\mu^* = 0.13]$(K)
10	1.05	21.5	18.6	16.1
20	0.77	31.4	15.5	12.4
50	0.41	56.4	3.0	1.4
100	0.39	59.9	2.3	0.9

Methods

The USPEX code[6,7] was used in conjunction with DFT to determine the most thermodynamically stable PN crystal structures for several different compositions. USPEX employs evolutionary algorithms to find the atomic structure with the lowest enthalpy at a given pressure, given knowledge *only* of the chemical composition of the unit cell. It has been employed with great success with many other systems at high pressure[43–46].

All structures were optimised with the CASTEP DFT code[47] at the GGA level, using the Perdew-Burke-Ernzerhof (PBE) exchange-correlation functional[48]. All lattice parameters and atomic positions were relaxed without constraints until forces varied by less than 0.05 eV Å^{-1} and energies by less than 1×10^{-5} eV between BFGS steps. SCF steps were considered to be converged when the total energy varied by less than 1×10^{-6} eV between steps. Electronic wavefunctions were expanded using a plane wave basis set with a cutoff of 350 eV, and core electrons ($1s^2$ in the case of N and

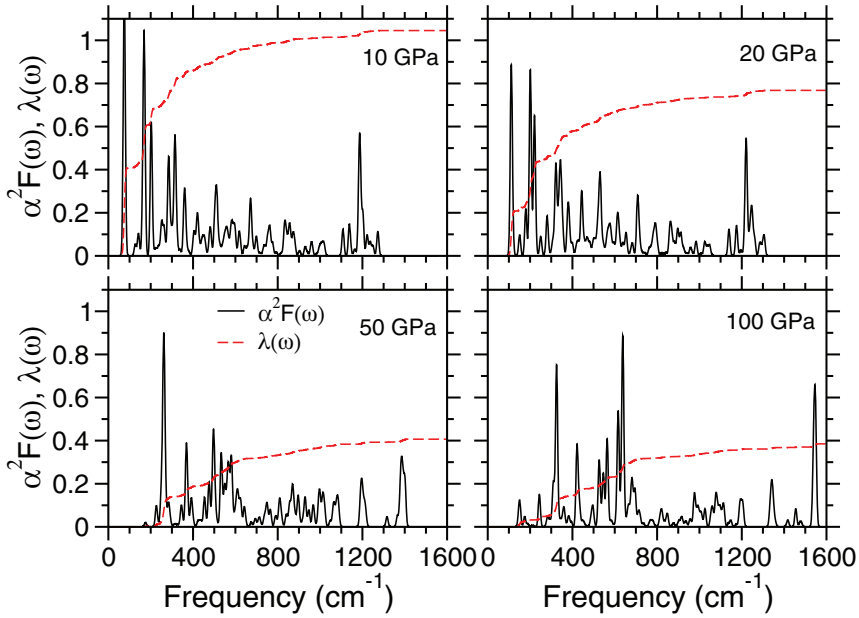

Figure 9 | Eliashberg function $\alpha^2F(\omega)$ and the integrated electron-phonon coupling constant $\lambda(\omega)=2\int_0^{\omega}\mathrm{d}\omega'\alpha^2F(\omega')/\omega'$ for the *Immm* phase at 10 GPa, 20 GPa, 50 GPa and 100 GPa.

$1s^22s^22p^6$ in the case of P) were represented with ultrasoft pseudopotentials. Monkhorst-Pack grids were generated per cell, using a spacing of $2\pi \times 0.05$ Å^{-1}. Ultrasoft pseudopotentials were employed with the intention of minimising calculation times; the nitrogen potential in particular had a core radius of 1.4 a_0, which may have resulted in core overlap in the case of structures with extremely short N−N bonds; however, enthalpies were compared with a hard reference pseudopotential with a 1.0 a_0 core radius, and the results found to be consistent.

Phonon and electron-phonon calculations were performed on the 16-atom primitive cell of the *Immm* skutterudite structure using density-functional perturbation theory (DFPT)[49] as implemented in the Quantum Espresso code[50]. Ultrasoft pseudopotentials, a plane wave cutoff of 60 Ry, a density cutoff of 600 Ry and a $4 \times 4 \times 4$ Monkhorst-Pack grid for the electronic integrations were used throughout. The cell was fully reoptimised using the new pseudopotentials, and selected conduction bands were projected onto maximally localised Wannier functions (MLWF) using the wannier90 code[51,52]. Phonon frequencies and electron-phonon coefficients were calculated on a $2 \times 2 \times 2$ **q**-point grid.

The Eliashberg functions of the electron-phonon coupling were calculated as

$$\alpha^2F(\omega)=\frac{1}{N(0)N_kN_q}\sum_{\mathbf{k}\mathbf{q}nm\mu}\left|g^{\mu}_{\mathbf{k}n,\mathbf{k}+\mathbf{q}m}\right|^2\delta(\epsilon_{\mathbf{k}n})\delta(\epsilon_{\mathbf{k}}+\mathbf{q}m)\times\delta\left(\omega-\omega_{\mu}(\mathbf{q})\right). \quad (1)$$

In Eq. (1) $g^{\mu}_{\mathbf{k}n,\mathbf{k}+\mathbf{q}m}=\sum_{s\alpha}\langle\mathbf{k}n|\delta V/\delta u^{s\alpha}(\mathbf{q})|\mathbf{k}+\mathbf{q}m\rangle\epsilon^{s\alpha}_{\mu}(\mathbf{q})\Big/\sqrt{2M_s\omega_{\mu}(\mathbf{q})}$ is the electron-phonon matrix element, where $|\mathbf{k}n\rangle$ is a Kohn-Sham state with energy $\epsilon_{\mathbf{k}n}$ measured from the Fermi level (ϵ_F), N_k and N_q are the number of electron and phonon momentum points used for the Brillouin zone sampling, $N(0)$ is the density of states per spin at ϵ_F, V is the self-consistent Kohn-Sham potential, $u^{s\alpha}(\mathbf{q})$ is the Fourier transformed displacement from equilibrium of atom s along Cartesian direction α, M_s is the mass of atom s, and $\omega_{\mu}(\mathbf{q})$ and $\epsilon^{s\alpha}_{\mu}(\mathbf{q})$ are respectively phonon frequency and polarisations with momentum **q**. A finer $12 \times 12 \times 12$ mesh was used in the sum over **k**-points in Eq. (1). Superconducting T_c values were estimated from the Allen-Dynes modified McMillan equation[53]:

$$T_c=\frac{\omega_{\log}}{1.2}\exp\left(-\frac{1.04(1+\lambda)}{\lambda-\mu*(1-0.62\lambda)}\right), \quad (2)$$

where the electron-phonon coupling constant is calculated as

$$\lambda=2\int_0^{\infty}\mathrm{d}\omega\frac{\alpha^2F(\omega)}{\omega}, \quad (3)$$

the logarithmic frequency average is $\omega_{\log}=\exp\left(\frac{2}{\lambda}\int_0^{\infty}\mathrm{d}\omega\frac{\alpha^2F(\omega)}{\omega}\ln\omega\right)$, and μ^* is the Coulomb pseudopotential parameter.

1. McMillan, P. F. New materials from high-pressure experiments. *Nature Mater* **1**, 19 (2002).
2. Solozhenko, V. L. & Gregoryanz, E. Synthesis of superhard materials. *Mater. Today* **8**, 44 (2005).
3. McMillan, P. F. High-pressure synthesis of materials. In *High-Pressure Crystallography: from fundamental phenomena to technological applications*, 373 (Springer, 2010).
4. Zerr, A., Miehe, G. & Riedel, R. Synthesis of cubic zirconium and hafnium nitride having Th_3P_4 structure. *Nature Mater.* **2**, 185 (2003).
5. Zhang, W. *et al.* Unexpected stable stoichiometries of sodium chlorides. *Science* **342**, 1502 (2013).
6. Oganov, A. R. & Glass, C. W. Crystal structure prediction using ab initio evolutionary techniques: principles and applications. *J. Chem. Phys.* **124**, 244704 (2006).
7. Oganov, A. R. & Glass, C. W. Evolutionary crystal structure prediction as a tool in materials design. *J. Phys.: Condens. Matter* **20**, 064210 (2008).
8. Pickard, C. J. & Needs, R. J. Ab initio random structure searching. *J. Phys.: Condens. Matter* **23**, 053201 (2011).
9. Wang, Y., Lv, J., Zhu, L. & Ma, Y. Crystal structure prediction via particle-swarm optimization. *Phys. Rev. B* **82**, 094116 (2010).
10. Buzea, C. & Robbie, K. Assembling the puzzle of superconducting elements: a review. *Supercond. Sci. Technol.* **18**, R1 (2005).
11. Xie, Y., Oganov, A. R. & Ma, Y. Novel high pressure structures and superconductivity of $CaLi_2$. *Phys. Rev. Lett.* **104**, 177005 (2010).
12. Martinez-Canales, M. *et al.* Novel structures and superconductivity of silane under pressure. *Phys. Rev. Lett.* **102**, 087005 (2009).
13. Gao, G. *et al.* Dissociation of methane under high pressure. *Proc. Natl. Acad. Sci. USA* **107**, 1317 (2010).
14. Zhu, L. *et al.* Substitutional alloy of bi and te at high pressure. *Phys. Rev. Lett.* **106**, 145501 (2011).
15. Errea, I., Martinez-Canales, M. & Bergara, A. Ab initio study of superconducting hexagonal Be_2Li under pressure. *Phys. Rev. B* **78**, 172501 (2008).
16. Raza, Z., Pickard, C. J., Pinilla, C. & Saitta, A. M. High energy density mixed polymeric phase from carbon monoxide and nitrogen. *Phys. Rev. Lett.* **111**, 235501 (2013).
17. Matthias, B. T. & Hulm, J. K. A search for new superconducting compounds. *Phys. Rev.* **87**, 799 (1952).
18. Yamanaka, S., Hotehama, K. & Kawaji, H. Superconductivity at 25.5 k in electron-doped layered hafnium nitride. *Nature Lett.* **392**, 580 (1998).
19. Wang, C. *et al.* First-principles calculations on the mechanical properties of niobium nitrides. *Solid State Commun.* **149**, 725 (2009).
20. Taguchi, Y., Kitora, A. & Iwasa, Y. Increase in t_c upon reduction of doping in Li_xZrNCl superconductors. *Phys. Rev. Lett.* **97**, 107001 (2006).
21. Sofo, J. O. & Mahan, G. D. Electronic structure of $CoSb_3$: a narrow-band-gap semiconductor. *Phys. Rev. B* **58**, 620 (1998).
22. Möchel, A. *et al.* Lattice dynamics in the $FeSb_3$ skutterudite. *Phys. Rev. B* **84**, 064302 (2011).
23. Meisner, G. P. Superconductivity and magnetic order in ternary rare earth transition metal phosphides. *Physica B + C* **108**, 763 (1981).
24. Slack, G. A. & Tsoukala, V. G. Some properties of semiconducting $IrSb_3$. *J. Appl. Phys.* **76**, 1665 (1994).

25. Jung, D., Whangbo, M. & Alvarex, S. Importance of the X_4 ring orbitals for the semiconducting, metallic, or superconducting properties of skutterudites MX_3 and RM_4X_{12}. *Inorg. Chem.* **29**, 2252 (1990).
26. Shirotani, I. *et al.* Superconductivity of filled skutterudites $LaRu_4As_{12}$ and $PrRu_4As_{12}$. *Phys. Rev. B* **56**, 7866 (1997).
27. Shirotani, I. *et al.* Superconductivity of the new skutterudite compound $La_xRh_4P_12$ at high pressure. *J. Phys.: Condens. Matter* **17**, 7353 (2005).
28. Bauer, E. *et al.* Superconductivity in novel ge-based skutterudites: $\{Sr,Ba\}Pt_4Ge_{12}$. *Phys. Rev. Lett.* **99**, 217001 (2007).
29. Bauer, E. *et al.* Superconductivity and spin fluctuations in $\{Th,U\}Pt_4Ge_{12}$ skutterudites. *Phys. Rev. B* **78**, 064516 (2008).
30. Bettermann, G., Krause, W., Riess, G. & Hofmann, T. Phosphorus compounds, inorganic. *Ullman's Encyclopedia of Industrial Chemistry* **27**, 1 (2012).
31. Schnick, W., Lu, J. & Krumeich, F. Phosphorus nitride P_3N_5: synthesis, spectroscopic and electron microscopic investigations. *Chem. Mater.* **8**, 281 (1996).
32. Horstmann, S., Irran, E. & Schnick, W. Synthesis and crystal structure of phosphorus (v) nitride α-P_3N_5. *Angew. Chem. Int. Ed.* **36**, 1873 (1997).
33. Landskron, K., Huppertz, H., Senker, J. & Schnick, W. High-pressure sysnthisis of γ-P_3N_5 at 11 gpa and 1500°c in a multianvil assembly: a binary phosphorus (v) nitride with a three-dimensional network structure from PN_4 tetrahedra and tetragonal PN_5 pyramids. *Angew. Chem. Int. Ed.* **40**, 2643 (2001).
34. Dong, J., Kinkhabwala, A. A. & McMillan, P. F. High-pressure polymorphism in phosphorus nitrides. *Phys. Status Solidi (B)* **241**, 2319 (2004).
35. Kroll, P. & Schnick, W. A density functional study of phosphorus nitride P_3N_5: refined geometries, properties and relative stability of α-P_3N_5 and γ-P_3N_5 and a further possible high-pressure phase δ-P_3N_5 with kyanite-type structure. *Chem. Eur. J.* **8**, 3530 (2002).
36. Pellicer-Porres, J., Saitta, A. M., Polian, A., Itié, J. P. & Hanfland, M. Six-fold-coordinated phosphorus by oxygen in $AlPO_4$ quartz homotype under pressure. *Nature Mater.* **6**, 698 (2007).
37. Llunell, M., Alemany, P., Alvarez, S., Vernes, A. & Zhukov, V. P. Electronic structure and bonding in skutterudite-type phosphides. *Phys. Rev. B* **53**, 10605 (1996).
38. Vining, C. B. Half-full glasses: the new black. *Nature Mater.* **7**, 765 (2008).
39. Mihaly, L. Crystal cages for clean coolers. *Nature* **395**, 839 (1998).
40. Mauri, F., Zakharov, O., de Gironcoli, S., Louie, S. G. & Cohen, M. L. Atomic structure of icosahedral B_4C boron carbide from a first principles analysis of nmr spectra. *Phys. Rev. Lett.* **77**, 1151 (1996).
41. Profeta, G. *et al.* Superconductivity in lithium, potassium, and aluminium under extreme pressure: a first-principles study. *Phys. Rev. Lett.* **96**, 047003 (2006).
42. Degtyareva, O. *et al.* Competition of charge-density waves and superconductivity in sulfur. *Phys. Rev. Lett.* **99**, 155505 (2007).
43. Oganov, A. R. *et al.* Ionic high-pressure form of elemental boron. *Nature* **457**, 863 (2009).
44. Ma, Y. *et al.* Transparent dense sodium. *Nature* **458**, 182 (2009).
45. Oganov, A. R. *et al.* Exotic behavior and crystal structures of calcium under pressure. *Proc. Natl. Acad. Sci. USA* **107**, 7646 (2010).
46. Oganov, A. R., Glass, C. W. & Ono, S. High-pressure phases of $CaCO_3$: crystal structure prediction and experiment. *Earth Planet Sci. Lett.* **241**, 95 (2006).
47. Clark, S. J. *et al.* First principles methods using castep. *Z. Kristall.* **220**, 567 (2005).
48. Perdew, J. P., Burke, K. & Ernzerhof, M. Generalized gradient approximation made simple. *Phys. Rev. Lett.* **77**, 3865 (1996).
49. Baroni, S., de Gironcoli, S., Dal Corso, A. & Giannozzi, P. Phonons and related crystal properties from density-functional perturbation theory. *Rev. Mod. Phys.* **73**, 515 (2001).
50. Giannozzi, P. *et al.* QUANTUM ESPRESSO: a modular and open-source software project for quantum simulations of materials. *J. Phys.: Condens. Matter* **21**, 395502 (2009).
51. Mostofi, A. A. *et al.* wannier90: A tool for obtaining maximally-localised wannier functions. *Comp. Phys. Comm.* **178**, 685 (2008).
52. Souza, I., Marzari, N. & Vanderbilt, D. Maximally localized wannier functions for entangled energy bands. *Phys. Rev. B* **65**, 035109 (2001).
53. Allen, P. B. & Dynes, R. C. Transition temperature of strong-coupled superconductors reanalyzed. *Phys. Rev. B* **12**, 905 (1975).

Acknowledgments

Z.R. and A.M.S. acknowledge the GENCI IDRIS French National supercomputing facility for CPU time (Project Grant No. 91387), and thank the French Agence Nationale de la Recherche (ANR) for support through Project No. ANR-2011-BS08-018. I.E. would like to acknowledge financial support from the Department of Education, Language Policy and Culture of the Basque Government (Grant No. BFI-2011-65). A.R.O. thanks the National Science Foundation (EAR-1114313, DMR-1231586), DARPA (Grants No. W31P4Q1210008 and W31P4Q1310005), the Government (No. 14.A12.31.003) and the Ministry of Education and Science of the Russian Federation (Project No. 8512) for financial support, and Foreign Talents Introduction and Academic Exchange Program (No. B08040).

Author contributions

Z.R. and I.E. performed the calculations, A.R.O. and A.M.S. contributed to the analysis. Z.R. and I.E. wrote the manuscript.

Additional information

Competing financial interests: The authors declare no competing financial interests.

How to cite this article: Raza, Z., Errea, I., Oganov, A.R. & Saitta, A.M. Novel superconducting skutterudite-type phosphorus nitride at high pressure from first-principles calculations. *Sci. Rep.* **4**, 5889; DOI:10.1038/srep05889 (2014).